ORNL/SPR-2021/2049

Evaluation of BISON's Transient Fission Gas Release Model on High-Burnup UO_2 MiniFuel

Nuclear Technology Research and Development

Prepared for
U.S. Department of Energy
Nuclear Technology R&D Program
Advanced Fuels Campaign
Amani Cheniour[1], Nathan Capps[1], Giovanni Pastore[2]
[1]Oak Ridge National Laboratory
[2]University of Tennessee, Knoxville

June 2021
M3FT-21OR020205022

ACKNOWLEDGEMENTS

This work was supported by the Advanced Fuels Campaign of the US Department of Energy Office of Nuclear Energy. The authors would like to express appreciation to Ian Greenquist (Oak Ridge National Laboratory) for his support in the review of this manuscript. Christian Petrie and Jacob Gorton (Oak Ridge National Laboratory) assisted with the development of the UO_2 MiniFuel test matrix.

SUMMARY

BISON's fission gas release (FGR) model was evaluated and tested over several hypothetical temperature transient conditions at high burnup and validated against FGR experimental data from an annealing test on high-burnup fuel. Diffusion-controlled FGR is accounted for in the model by including several physical mechanisms such as the diffusion of fission gas to grain faces, grain boundary sweeping, grain growth, and intergranular bubble growth. Under temperature variations, the development of microcracks at grain faces increases FGR. Nevertheless, a fraction of the FGR during temperature transients such as loss-of-coolant accident (LOCA) can be a result of different mechanisms (in particular, fuel fragmentation) and present an important dependency on local burnup and high burnup structure formation. This report documents a systematic study conducted to investigate the performance and necessary developments of the existing BISON fission gas release model for the analysis of LOCA-type transients. The model is applied to a UO_2 Miniature Fuel (MiniFuel) example and shows an overall good qualitative agreement with experimental observations on FGR during annealing tests under different temperature conditions. It also accounts well for microstructural effects on FGR. When quantitatively compared with FGR data from previously irradiated 103 MWd/kgU UO_2 discs under thermal annealing, the model shows a less satisfactory agreement with the experimental data. Finally, a UO_2 MiniFuel test matrix is proposed to help to improve and validate the current FGR model in BISON.

CONTENTS

FIGURES

TABLES

ACRONYMS

FGBR	fission gas burst release
FGR	fission gas release
GB	grain boundary
HBS	high burnup structure
HFIR	High Flux Isotope Reactor
IG	intragranular
LHR	linear heat rate
LOCA	loss-of-coolant accident
LWR	light water reactor
MiniFuel	Miniature Fuel
MOOSE	Multiphysics Object-Oriented Simulation Environment
ORNL	Oak Ridge National Laboratory
SIFGRS	Simple Integrated Fission Gas Release and Swelling

EVALUATION OF BISON'S TRANSIENT FISSION GAS RELEASE MODEL ON HIGH-BURNUP UO_2 MINIFUEL

1. INTRODUCTION

Miniature Fuel (MiniFuel) has recently emerged as a new fuel testing design to provide insight into fuel behavior under accelerated and well-controlled conditions [1-5], similarly to the Halden disk concept [6]. It was developed at Oak Ridge National Laboratory (ORNL) and is approximately 1,000 times smaller than light-water reactor (LWR) fuel pellets [1]. Accompanied by modeling and simulation, the MiniFuel design can potentially accelerate the development of new fuel concepts and accident-tolerant fuels. Because of its very small size, the MiniFuel sample has a uniform temperature and very low thermal gradients [1]. The main advantage of this design is to hold the temperature constant while increasing the fission rate of the fuel above that observed in an LWR, thus accelerating burnup accumulation. MiniFuel uses depleted or natural uranium, which reduces its fabrication cost [1]. The purpose of this milestone report is to systematically evaluate the current transient fission gas release model in the fuel performance code BISON by applying it on a high-burnup MiniFuel sample and validating it against experimental data for temperature transient conditions. The model results are then used to support the development of a MiniFuel irradiation test matrix for evaluating fission gas release (FGR) in steady-state and temperature transient conditions.

Under normal LWR irradiation conditions, FGR results in a degradation of the heat transfer across the gap between the fuel pellet and the cladding. As fission gas accumulates in the gap, the gap thermal conductance is reduced, consequently increasing the fuel temperature. This increased temperature results in higher diffusion rates of fission gas atoms across the fuel and therefore more FGR. Xenon and krypton are the main gaseous fission products constituting fission gas. Because of its low solubility in the UO_2 matrix, fission gas is often present in compounds with uranium vacancies, eventually leading to the formation of bubbles [7-8]. This process reduces the overall energy of the material and is therefore thermodynamically favorable. Like intragranular bubbles, grain face bubbles are a preferred location for fission gas storage. Grain face bubbles grow, interconnect, and coalesce as a result of the continuous segregation of fission gas at grain boundaries. Ultimately, pathways for FGR to the free volume are created through bubble interconnection along grain edges [7-9].

Under transient conditions, FGR in high-burnup fuel increases compared with steady-state conditions because of the rapid temperature increase and the highly pressurized grain face bubbles, resulting in grain boundary separation. During loss-of-coolant accident (LOCA) transients, fission gas bubble pressurization can lead to fine fragmentation of the fuel [10]. This results in a phenomenon of rapid FGR called *fission gas burst release* (FGBR). In fact, both the diffusion of fission gas and grain face microcracking processes are accelerated if the high-burnup structure (HBS) has already formed. HBS is characterized by the formation of small subgrains, which reduces the distance to grain boundaries [11]. Large overpressurized bubbles are thus created, exerting pressure on the surrounding grains. HBS starts forming at the rim of the fuel pellet and extends toward the center as burnup increases. The development of HBS results in more FGR during transients [10].

Several thermal annealing experiments on high-burnup fuel have been conducted to understand FGR conditions during LOCA-type scenarios. Une et al. [10] determined that the fuel burnup, heating rate, and terminal temperature influence the FGR rate. The study emphasized the impact of both the heating rate and the presence of HBS. The authors found that diffusion-controlled FGR is dominant at low heating rates, whereas fragmentation and microcracking at grain faces caused high FGR at high heating rates above a certain temperature. Conclusions on the mechanisms behind FGR during thermal annealing were

also obtained from a previous study by Pontillon et al. [12] using fuel samples irradiated in a pressurized water reactor. Additionally, it was found that a higher fractional release is obtained with more fuel cycles and that the onset of FGBR was obtained at different critical temperatures, depending on the burnup and temperature ramp.

During the temperature sequence, two FGR peaks were observed. The authors suggest that the low temperature release is attributed to microcracking, whereas the high temperature peak is the result of bubble interconnection. Another annealing study on very high-burnup fuel by Hiernaut et al. [13] confirms the major role that microstructure changes at high burnup have in the release process. A later investigation by Marcet et al. [14] revealed that the HBS zone released up to twice the fission gas amount the fuel central zone released during the LOCA-type transient.

A thorough assessment of fuel performance, and most specifically FGR, requires significant experimental efforts to understand the physical mechanisms. Additionally, FGR model development, verification, and validation are essential for an improved understanding of FGR. BISON has emerged as a powerful multiphysics fuel performance code, and it includes a physics-based FGR model for UO_2 [15–17]. To assess BISON's FGR predictions using the Simple Integrated Fission Gas Release and Swelling (SIFGRS) model, this report is structured as follows:

- A short description of the MiniFuel experiment vehicle and recent irradiation experiments is provided.
- A summary of the FGR mechanisms included in the SIFGRS model is presented.
- An assessment of the impact of temperature and burnup conditions and microstructural features on FGR in MiniFuel using BISON is performed.
- SIFGRS is validated against experimental data from the literature.

This study focuses mainly on UO_2 fuel but will also investigate the impact of adding chromium as a UO_2 dopant on FGR. FGR modeling is nevertheless relevant for other nuclear fuel choices such as U_3Si_2 and UN.

2. MINIFUEL EXPERIMENT VEHICLE

The MiniFuel irradiation design is detailed in the paper by Petrie et al. [1] and is comprised of a basket of up to nine sealed targets. Each target has six capsules, which contain the fuel specimen inside a cup surrounded by a filler material (such as molybdenum) and a SiC temperature monitor to measure the irradiation temperature using dilatometry during post-irradiation analysis. Three radial positions can be used to place three targets superimposed axially. Two of the three radial positions are at the same distance from the core center (radial positions 2 and 3) and the last position is farther from the core (radial position 1). The MiniFuel vehicle can be placed in the inner small vertical experiment facility of the High Flux Isotope Reactor (HFIR) [1]. Thanks to the plutonium-239 breeding capability of HFIR, natural or low-enriched uranium-235 can be used in the fuel, which significantly reduces the fabrication cost and time requirements [1]. The high irradiation flux provided by HFIR (approximately 2×10^{15} n/cm^2/s for thermal neutrons) allows for rapid fuel burnup, therefore significantly shortening the irradiation timeline and potentially accelerating fuel concept design and development [1]. As a result of the small size of the fuel specimen, most of the heat is generated through gamma heating in the materials surrounding the fuel. This allows for a decoupling of the fuel temperature from the fission rate, and hence better control of the experimental conditions [1]. Overall, compared to integral fuel tests, MiniFuel tests can potentially provide more detailed information on irradiation-induced mechanisms such as fission gas release in a shorter time and with less fabrication cost and effort than separate effects testing [1-4].

Different design options were developed for the fuel capsule to accommodate kernels of two different sizes, TRISO fuel, and fuel disks. MiniFuel irradiation experiments have already been performed on low-enrichment UN kernels with low carbon amounts as well as UN TRISO particles at low irradiation temperature and burnup [2, 3]. Irradiation temperature and fuel burnup measurements were compared to simulation results obtained using radiation transport codes and finite-element simulations [2]. Post-irradiation evaluation of the fuel specimen involved FGR measurement using a puncture test [2]. However, FGR is low in the UN kernels and very limited in the UN TRISO fuel as a result of the low burnup (up to approximately 10 MWd/kgU) reached after the irradiation period of 68 full power days. Fuel microstructure evaluation showed limited changes due to irradiation, which is also consistent with the low fuel burnup.

In addition to UN kernels and UN TRISO particles, monolithic MiniFuel capsules of UO_2 and U_3Si_2 disks have been fabricated and prepared to be irradiated in HFIR at low irradiation temperature [4]. The target burnup is 8 to 10 MWd/kgU for UO_2 and 28 to 40 MWd/kgU for U_3Si_2, an accident tolerant fuel [4]. Fission gas release will be measured in post-irradiation examination of both fuel types.

3. BISON FISSION GAS RELEASE MODEL

BISON is a nuclear fuel performance code based on the Multiphysics Object-Oriented Simulation Environment (MOOSE), a finite-element code developed at Idaho National Laboratory [18]. MOOSE is a powerful simulation tool that allows for the coupling of different nonlinear partial differential equations for multiphysics problems. BISON has been used to simulate the thermomechanical behavior of nuclear fuel and cladding materials at the engineering scale [16]. Relevant physical models such as thermal expansion, creep, swelling, and FGR have been implemented in BISON for a variety of fuels and claddings [17]. The validation of BISON has been addressed in several published manuscripts, which demonstrated its good predictive capabilities [19-21].

The SIFGRS model in BISON uses several physics-based models from the literature to compute UO_2 FGR and swelling resulting from specific effects [15, 17] such as the microstructural features (e.g., grain size, porosity, bubble density), fuel burnup, and temperature conditions. The SIFGRS model addresses the following phenomena that lead to FGR:

- intragranular fission gas migration,
- intergranular fission gas migration,
- an athermal release mechanism,
- grain boundary sweeping, and
- temperature-dependent microcracking.

It was recently employed to model FGR in power ramp tests, showing a fair agreement with experimental data [22, 23].

The transient model calculates the grain faces fractional coverage F affected by the diffusion of gas out of grain faces (gas depletion) and microcracking at grain boundaries. The diffusional contribution is determined by bubble growth and a threshold in the grain boundary coverage. The microcracking contribution corresponds to gas depletion of a fraction of the grain faces and is modeled as a reduction of the fractional coverage (i.e., the fraction of grain surface occupied by gas bubbles). Such a reduction is calculated as dependent on temperature variations, with the evolving fraction of intact grain faces f governed by

$$\frac{df}{dt} = -\frac{dm}{dt} f, \tag{1}$$

where m is an empirically derived temperature-dependent sigmoid function [15, 17]

$$m(T) = 1 - \left[1 + Qexp\left(s\frac{T - T_{cent}}{T_{span}}\right)\right]^{-\frac{1}{Q}}, \tag{2}$$

and where T_{cent} is the central fuel temperature set to 1773 K and can be adjusted to account for the current burnup, T_{span} is related to the temperature-domain width of the phenomenon and is set to 5 K, and Q and s are model parameters [17]. Q is set to 33, and s to 1 for heating transients and to -1 for cooling transients. T_{cent} was introduced because experimental data showed that FGR bursts reach a maximum value at a burnup-dependent central temperature [17, 24].

The model assumes a saturation coverage as a function of the rate of microcracking and microcrack healing [15, 20]. The latter rate is dependent on the local temperature and is therefore sensitive to temperature ramps. Additional details about the FGR model can be found in the literature [15, 22, 23, 25].

4. EVALUATION OF THE FGR MODEL IN TRANSIENT SCENARIOS

In this section, BISON is used to calculate the fractional release of fission gas for high-burnup fuels in steady-state conditions followed by a temperature transient. The 3D MiniFuel mesh used in this work is shown in Figure 1 and consists of a quarter of two disks: the fuel disk and the refractory metal cup disk, separated by a gap. A MiniFuel disk geometry is used to avoid thermal gradients and to identify the effects of separate quantities and parameters in the model on transient FGR. Furthermore, modeling MiniFuel helps to develop a MiniFuel irradiation test matrix to evaluate FGR and microstructure evolution at high burnup and in temperature transient conditions.

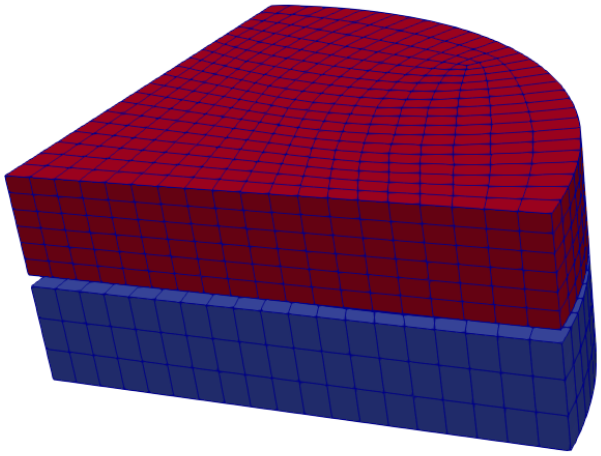

Figure 1. MiniFuel mesh and geometry showing the fuel disk in red and the refractory metal cup disk in blue.

The disk radius is set to 1.64 mm and its thickness is set to 0.319 mm. The metal disk is considered as the cladding. Under steady-state conditions, the cladding temperature was set to 500°C. However, to obtain significant FGR, the fuel temperature was varied by changing the conductance of the gap to enable different fission gas diffusion rates and, more generally, to investigate the impact of the irradiation temperature on FGR in UO_2. Steady-state conditions were applied until a specified final burnup is reached. Then, a time-dependent temperature profile was applied to the outer cladding surface to apply a temperature transient scenario similar to LOCA. The linear heat rate (LHR) is initially set to 8805.78 W/m and rapidly reduces to 616.4 W/m once the cladding temperature starts to increase. The power shutdown decreases the fuel temperature, but the boundary condition applied on the cladding temperature causes the temperature to go back up: this is an example of a temperature transient. Figure 2 shows the evolution of the peak fuel and cladding temperatures. This section documents the application of BISON's FGR model to various temperature transient problems to evaluate its performance and the effects of temperature conditions, burnup, and microstructural features on FGR.

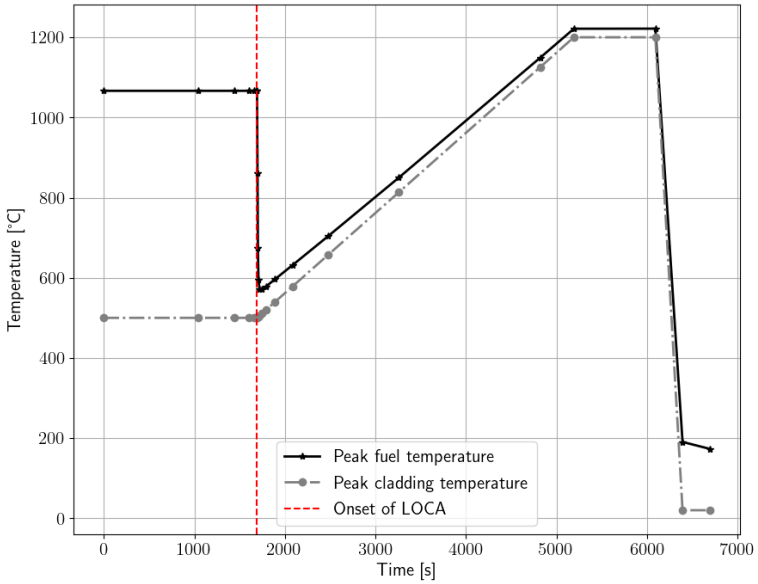

Figure 2. Fuel and cladding temperature variations before and after the temperature transient conditions.

4.1 Temperature Transient Conditions

4.1.1 Fuel Temperature and Burnup

Because FGR is mainly controlled by the fuel temperature, the gap thermal properties are modified to produce five different fuel temperature values ranging from 577 to 1,059°C. The heating rate is set 0.2°C/s and the burnup at the transient onset is set to 90 MWd/kgU. The simulation parameters are summarized in

Table 1. The average grain size is 10 μm. The cladding temperature is raised from 500 to 1200°C, held for 15 minutes, and then decreased to room temperature.

Table 1. Simulation parameters to study FGR's dependence on fuel temperature

Parameter	Value
Fuel temperature range	577 to 1059°C
Heating rate	0.2°C/s
Burnup at transient onset	90 MWd/kgU
Average grain size	10 µm

Figure 3 shows plots of the transient FGR depending on the fuel irradiation temperature T_f before the transient. The cladding temperature T_c is also shown in Figure 3. The power shutdown leading to a fuel temperature decrease is accompanied by a small peak in the FGR fraction from the transient model. The magnitude of the increase is related to the fission gas available as well as the fuel temperature [22, 23]. Low fuel temperatures result in a slow increase of FGR as the cladding temperature approaches 1200°C because more diffusion-controlled FGR occurs. This increase is followed by a steeper positive slope when the sample is cooled down, which is also as a result of the transient model. Figure 3 also shows that the transient FGR behavior can be different depending on the irradiation temperature. For instance, at $T_f = 848$°C, less FGR is predicted than at $T_f = 577$°C or at $T_f = 1057$°C by the end of the transient. The diffusion-based model includes several mechanisms (as previously discussed) that result in these differences in the transient FGR as a function of fuel temperature.

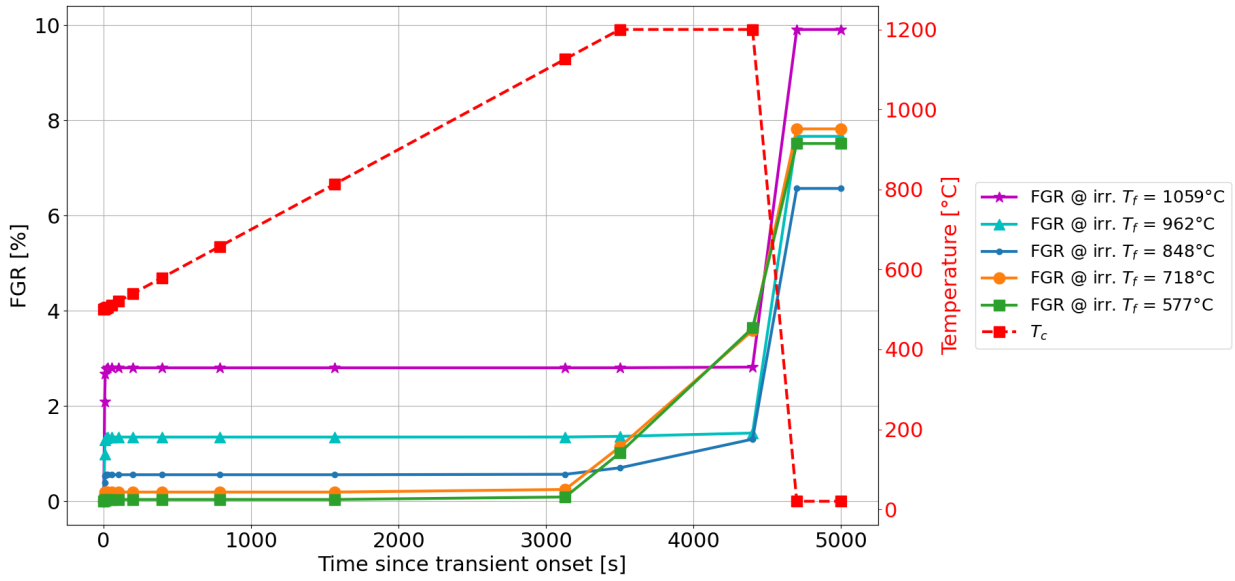

Figure 3. Transient fission gas release depending on the steady-state peak fuel temperature (irr. T_f) and variation of the cladding temperature T_c.

As the fission gas diffusion rate increases rapidly, grain face bubbles grow faster, which leads to more interconnection and release to the surface. This explains the change in the FGR rate at approximately $t = 3200$ s. The following sharp increase in FGR is related to the temperature variation–driven

microcracking FGR, and is the result of the overpressurization of intergranular bubbles. However, the model is only sensitive to temperature variations and does not account for the bubble pressure. The cumulative FGR during steady-state then transient conditions becomes more significant with higher fuel temperatures, reaching up to 51% for an initial fuel temperature of 1059°C. Overall, the evolution of the FGR fraction follows a consistent behavior regardless of the fuel temperature before the transient. This behavior is expected and presents a fair agreement with the trend observed in experimental studies [12]. The results of a quantitative validation study are provided in the following section.

Next, the impact of fuel burnup on FGR is addressed. BISON's model captures the impact of fuel temperature on fission gas diffusion and release. It has also been shown that the model correctly predicts that the release fraction grows with burnup in steady-state conditions. The next set of simulations evaluates the transient FGR model at different burnup levels ranging from 70 to 150 MWd/kgU, starting with two distinct steady-state peak fuel temperatures. Table 2 shows the fractions of FGR before and after the temperature transient at different burnup and temperature conditions. The lower temperature case (T_f = 577°C) shows that less fission gas is released with burnup, which is contrary to the trend obtained from the higher temperature case. Figure 4 shows the evolution of FGR for each burnup value at both steady-state fuel temperatures. In Figure 4a, the diffusion mechanism is more dominant since the steady-state fuel temperature is lower. When the temperature is high (T_f = 1059°C), this effect is not apparent, as demonstrated by Figure 4b, because transient FGR is mainly controlled by microcracking. This result is justified by the evolution of fission gas available at grain boundaries during the transient, as will be discussed further in this report (Figure 12).

Although the microcracking model accounts for temperature variations, it does not consider the formation of HBS at such high burnups. Because HBS is more vulnerable to cracking during transients, its presence raises the amount of released gas under such conditions. The presence of submicron grains in HBS allows for faster diffusion to grain boundaries and bubbles [26, 27]. The overpressurized bubbles release a significant quantity of fission gas as a result of the increasing temperature. Figure 4b shows that the change in FGR is quite similar across all the burnups studied. This result is expected because the change is exclusively related to the temperature variation, which did not change for all five burnup cases. However, this result does not match experimental observations in which microcracking is more significant at higher burnups [10].

Table 2. Cumulative FGR for initial average peak fuel temperatures and high-burnup values predicted by BISON

	Burnup [MWd/kgU]	**70**	**90**	**110**	**130**	**150**
T_f = 577°C	Steady-state FGR [%]	0.00	4.71	9.01	12.34	15.06
	Transient FGR [%]	7.61	7.52	6.75	5.84	5.24
	Total FGR [%]	7.61	12.23	15.76	18.18	20.30
T_f = 1,059°C	Steady-state FGR [%]	37.57	41.09	43.73	45.92	48.08
	Transient FGR [%]	9.58	9.91	10.13	10.29	10.47
	Total FGR [%]	47.15	51.00	53.86	56.21	58.55

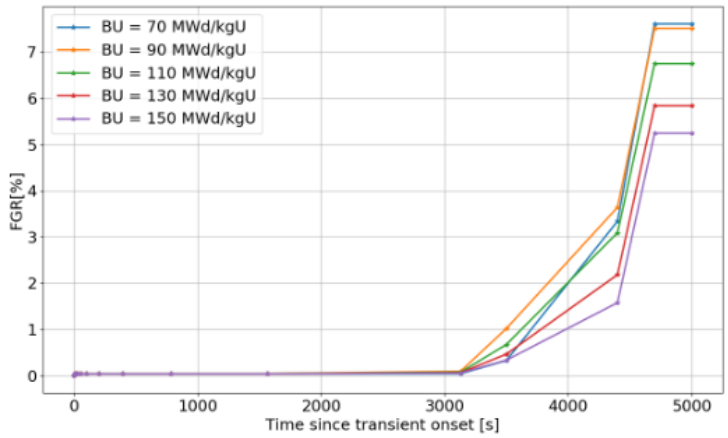

(a) T_f = 577°C before transient

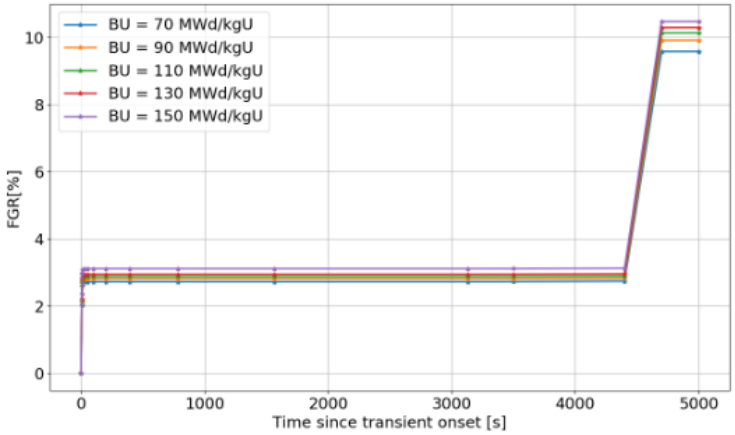

(b) T_f = 1059°C before transient

Figure 4. Transient FGR evolution with burnup.

4.1.2 Heating Rate

The heating rate is expected to affect the total FGR because it controls the available time for bubble growth and interconnection in the model [10]. Table 3 shows that higher heating rates can reduce the total FGR during the temperature transient, which agrees with experimental observations [10, 12]. The final burnup is 90 MWd/kgU. A more detailed representation of this result can be seen in Figure 5, which shows that the FGR fraction before cooling is the lowest when the highest heating rate 50°C/s is applied.

Table 3. Transient FGR under temperature transient conditions at 90 MWd/kgU at different heating rates as predicted by BISON

Heating rate [°C/s]	0.2	10	20	50
Transient FGR [%]	9.91	9.74	9.55	8.22

The amounts in mole of intragranular and intergranular fission gas during the transient are shown in Figure 6 for two heating rates: 0.2 and 50°C/s. The figure shows a significant overall drop in intergranular fission gas with time, and the highest residual amount corresponds to the highest heating rate. For both cases, the overall change in intragranular fission gas is negligible compared with the change in intergranular fission gas, which is consistent with previous experimental data [12]. Note that if higher fuel temperatures are used in the simulation, then the change in intragranular fission gas concentration will be more pronounced. The intergranular fission gas portion is very sensitive to rapid temperature changes for both heating rates. The initial drop in this quantity is explained by the decrease in the fuel temperature as a result of power loss. With a heating rate of 50°C/s, the fuel temperature rapidly goes back up, resulting in a less significant drop in intergranular fission gas.

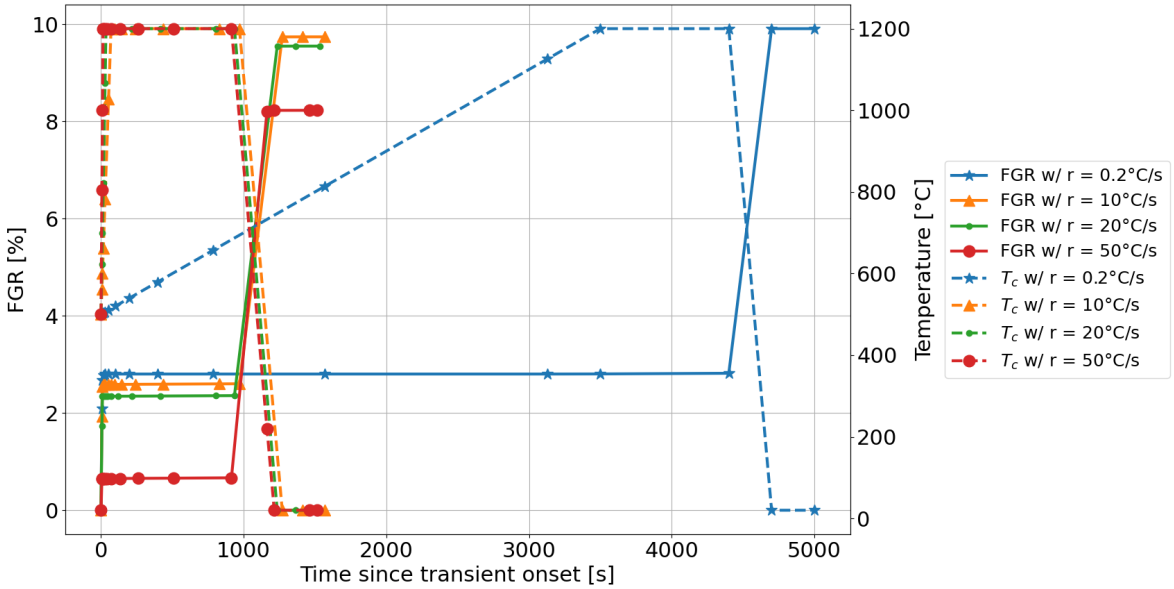

Figure 5. Transient FGR and cladding temperature T_c change with heating rate *r*.

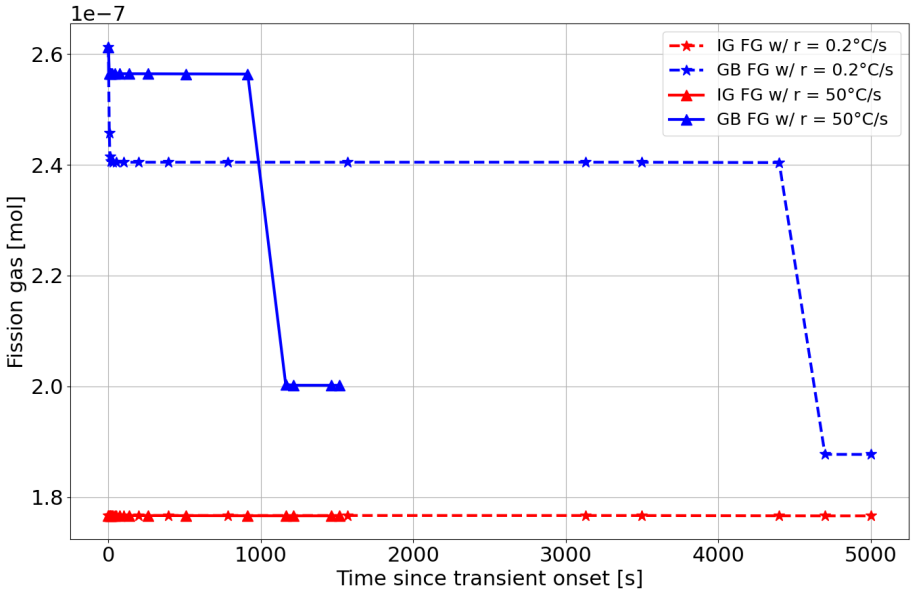

Figure 6. Fission gas accumulated inside grains (IG) and at grain boundaries (GB) in moles depending on the heating rate *r*.

4.1.3 Terminal Temperature and Hold Time

The terminal temperature is expected to change the release fraction as both FGR mechanisms are highly temperature dependent. To evaluate the model's performance in this case, the terminal temperature was increased to 1400°C. At this temperature, the model predicts a total release fraction of 62.08% with an 11.08% gain compared with the previous result recorded at a terminal temperature of 1200°C.

The hold time defines the duration for which the fuel temperature is at its maximum value during the transient. From an FGR perspective, increasing the hold time leads to further bubble growth and coalescence, thus more release. Any effects on the pressure inside rim bubbles is not included; therefore, the simulation predicts a decrease in intragranular fission gas as the hold time increases from 10 to 15 minutes. During the hold time, no microcracking effect on FGR is captured because the fuel temperature time derivative equals zero. Pontillon et al. [12] measured the FGR fractions for annealing tests A-2 and A-2bis applied on previously irradiated LWR fuel. Hold times of 10 and 0 minutes were used, respectively, and the authors determined that more FGR occurred in the A2 case [12]. For a better comparison, two thermal annealing simulations using a 3D LWR three-pellet geometry was performed to demonstrate FGR rates in LWR conditions. The 6-cycle burnup and temperature transient conditions described by Pontillon et al. [12] for tests A-2 and A-2bis were applied for comparison, and 11.6% and 11.1% FGR were obtained, respectively [12]. Figure 7 shows the FGR results obtained. The FGR model performs as expected in the constant temperature region, where some release occurs because of diffusion-controlled FGR. However, the model predicts lower transient FGR fractions in both cases. The experimental values in the paper by Pontillon et al. [12] are close in both tests; however, in the paper by Une et al. [10] , higher heating rates are used for comparison, which shows a more significant difference in the results. Figure 11 in the paper by Une et al. [10] suggests that lower heating rates increase FGR for the same terminal temperature, which is consistent with BISON's model prediction.

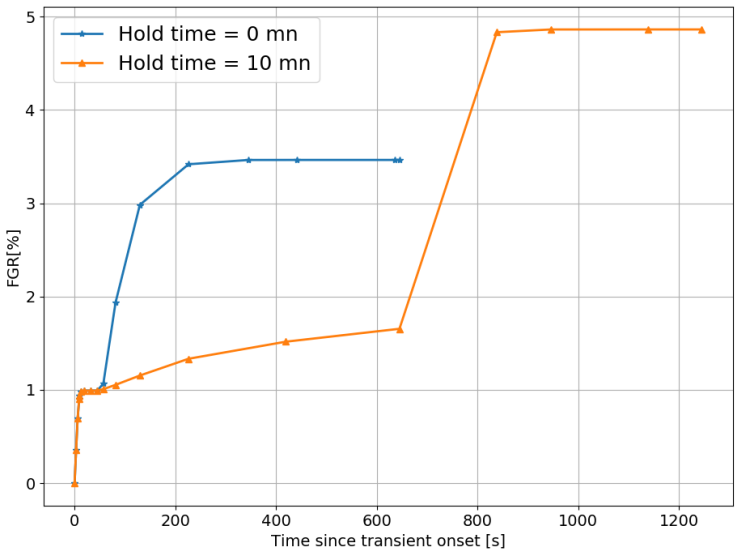

Figure 7. BISON transient FGR simulation results using the burnup and thermal annealing conditions of tests A-2 and A-2bis described in Pontillon et al. [12].

4.2 Microstructural Effects

The nucleation and growth of fission gas bubbles result from the diffusion and accumulation of fission gas atoms and uranium vacancies. Larger grains reduce FGR as the diffusion distance to grain boundaries and grain face bubbles grows. The SIFGRS model calculates FGR based on physical mechanisms at the microstructure level, such as bubble growth and coalescence, and microcracking at grain boundaries. This subsection qualitatively assesses microstructural effects on BISON's FGR calculation at high burnup in temperature transient conditions. Several microstructural features and phenomena are addressed here. Additionally, FGR in chromium-doped UO_2 is evaluated for a specified grain size.

The following simulations use the same MiniFuel mesh and geometry previously described. The outer cladding surface was heated from 500 to 1,200°C at a rate of 0.2°C/s, held for 15 minutes, and then cooled down to 20°C.

4.2.1 Grain Size

FGR is evaluated for different grain sizes in the UO_2 fuel matrix and steady-state fuel temperatures. The aim of this work is to quantify the loss in FGR with increasing grain size. Temperature transient conditions are added at the end of the steady-state simulation at 90 MWd/kgU. The grain size evolution during the simulation is shown in Figure 8 for a steady-state fuel temperature T_f = 1,059°C. The grain size remains approximately constant under the temperature transient conditions. The grain growth rate is computed based on the model in the paper by Ainscough et al. [28]. Figure 9 presents the simulation results for ten grain sizes ranging from 5 to 50 µm. BISON predicts a significant drop in FGR at higher fuel temperatures as the grain size increases. For instance, for a steady-state fuel temperature of 1,059°C, the total FGR decreases from approximately 63 to 15% as the grain size changes from 5 to 50 µm. At lower temperatures, this difference is less pronounced but remains significant.

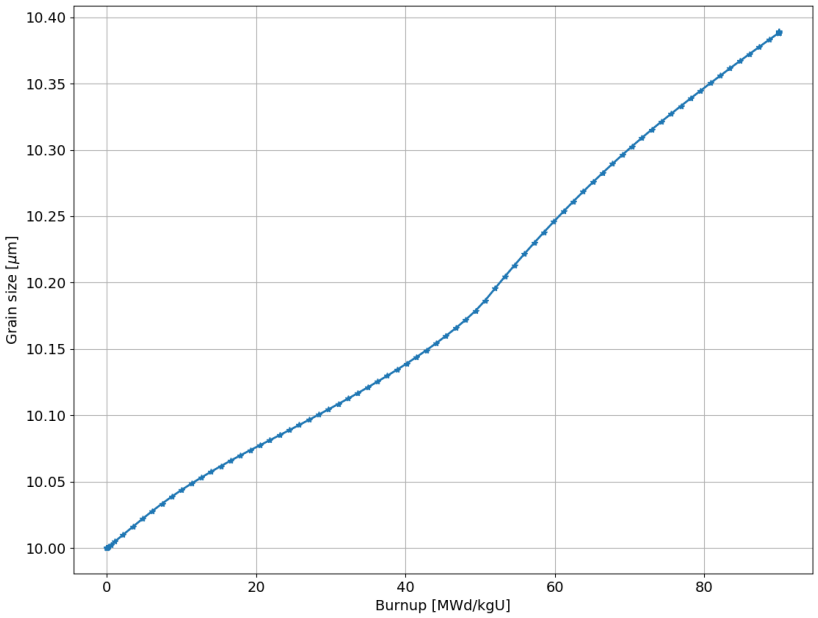

Figure 8. Average grain size evolution with burnup with steady-state fuel temperature T_f = 1,057°C.

The FGR at all temperatures begins to saturate for larger grain sizes. This also implies a smaller rate of change in FGR as the grain size evolves across the different simulations. A similar trend in FGR evolution with grain size was observed in steady-state conditions using BISON. This trend is confirmed by the diffusion theory, where larger grain sizes increase the distance that fission gas atoms are required to travel before reaching grain boundaries and potentially forming bubbles. The results also show that grain size and diffusion-controlled FGR have a significant impact on the total FGR at high burnup calculated according to BISON's model.

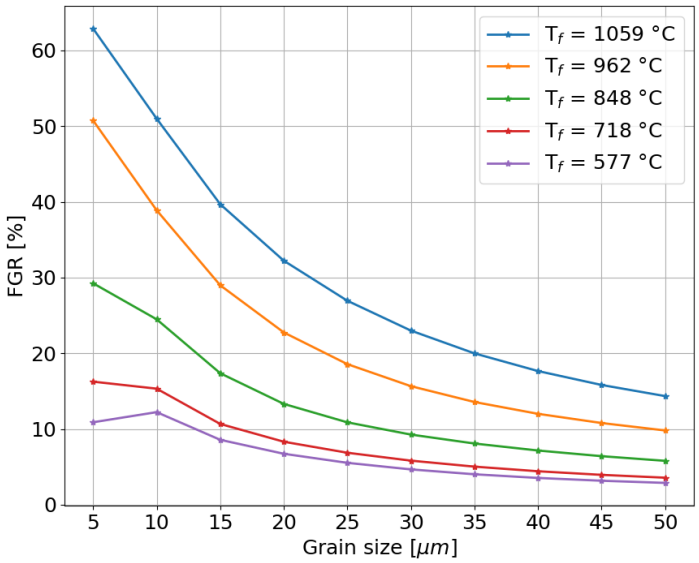

Figure 9. Total FGR depending on the grain size and irradiation temperature.

4.2.2 Xenon and Uranium Vacancy Diffusion

Other crucial parameters in the determination of the microstructural behavior and fuel performance of UO_2 are the diffusion coefficients of xenon and uranium vacancy because they are strongly correlated to diffusion-controlled FGR. These properties have been measured by several experiments and computed through atomistic-scale simulations in the literature [29, 32]. In fact, different experiments showed largely different values of these properties for given temperature ranges. The resulting uncertainty motivates the investigation of the impact of this diffusivity on FGR.

The xenon diffusion term in BISON is computed following the formulation by Turnbull et al. for an effective diffusivity based on the fission rate and temperature [32]. Any variation of this parameter impacts FGR to some extent. The xenon diffusion coefficient was multiplied by a factor ranging from 1 to 100. The final burnup is 90 MWd/kgU. Figure 10 shows the variation of FGR during the transient depending on the diffusion factor's value. For intragranular diffusion shown in Figure 10a, FGR increases when the diffusivity changes by a factor of 10 or 100. FGR reaches a saturation level rapidly at higher intragranular diffusion rates since fission gas generation cannot compete with FGR anymore. However, the change in FGR is very limited; there is a less than 2.3% FGR increase for the highest diffusion coefficient compared to the original diffusivity.

In the BISON FGR model, the vacancy diffusion coefficient is used principally to determine the number, density, and size of grain face bubbles. Therefore, it plays an important role in this model. This parameter is also difficult to estimate through experiments, which adds uncertainty to the diffusion-based model. To investigate such uncertainty, the vacancy diffusion coefficient was also increased by a factor of 10 and 100, independently of the previous xenon diffusion related simulations. Figure 10b presents the results for intergranular diffusion. Like the intragranular diffusion case, FGR is almost unaffected by the variation in vacancy diffusivity.

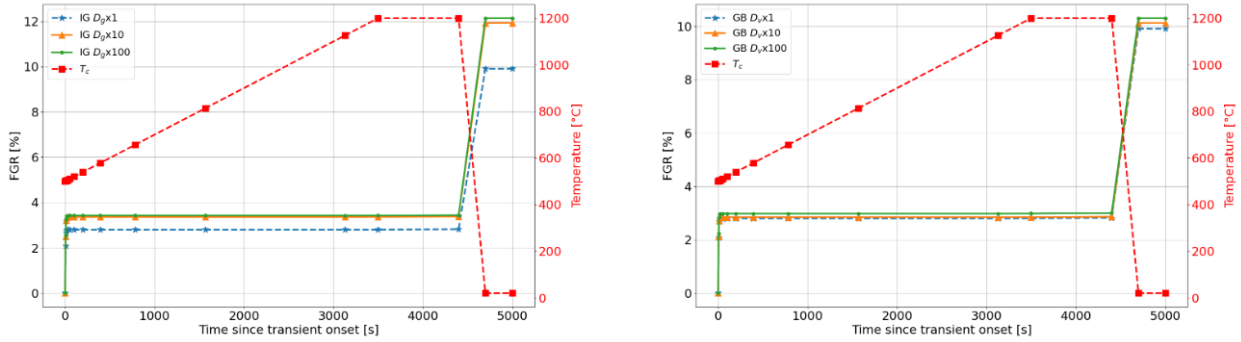

(a) Intragranular xenon diffusion (IG) **(b) Grain boundary vacancy diffusion (GB)**

Figure 10. Effects of (a) xenon and (b) uranium vacancy diffusion coefficients on FGR during transient.

4.2.3 Dopant Addition

Chromium-doped UO_2 has been investigated as a potential LWR fuel because of its higher fuel density and the larger grain size that is obtained after powder sintering. The main advantages of such fuel aspects are a decrease in FGR (as shown previously with larger grains) and a reduction in possible interactions with the cladding through reduced swelling. Doped fuels are being studied aggressively to evaluate their performance in steady-state and transient conditions [33]. BISON can account for the presence of chromium in UO_2 in its FGR model by modifying the uranium vacancy diffusion coefficient. This method

is justified by recent atomistic-scale simulations that determined the impact of different dopants on the activation energy of uranium vacancies and their diffusivity [34]. Several possible values are given in the literature for vacancy diffusion in chromium-doped UO_2. In the following results, the diffusion term is corrected as suggested by Cooper et al. [34, 35] by accounting for the relative change in vacancy concentration relative to the undoped fuel case. However, the calculated vacancy concentration in chromium-doped UO_2 in the paper by Cooper et al. [34] becomes different from that in undoped UO_2 at temperatures higher than approximately 1800 K; therefore, the uranium vacancy diffusion coefficient effectively remains the same as for undoped fuel in this work. The calculated FGR of the doped fuel was compared with that of undoped fuel in BISON. The chosen average grain size was 30 μm; however, doped fuels can have larger grain sizes, potentially reaching 50 μm [33]. Table 4 shows the total FGR during the transient in addition to the FGR before the transient. The result shows a significant drop in FGR as a result of the dopant addition, as expected, which is consistent with experimental results [33]. Arborelius et al. [33] showed that the ADOPT doped fuel reduces FGR by up to 50% compared to undoped UO_2. In this case, with an average grain size of only 30 μm, FGR was reduced by approximately 27% in steady-state conditions and 6% in temperature transient conditions.

Table 4. Cumulative fission gas release for Cr-doped and undoped UO_2 predicted by BISON

Fuel type	Undoped UO_2	Cr-doped UO_2
Steady-state FGR [%]	41.09	13.89
Transient FGR [%]	9.91	3.59
Total FGR [%]	51.00	17.48

4.2.4 Fission Gas Bubbles

The simulation setup in the evaluation of FGR dependency on fuel burnup presented in Section 4.1.1 is also used to assess the microstructural changes during the transient, in which irradiation temperatures of 577 and 1,059°C are used, and in which burnup varies from 70 to 150 MWd/kgU.

4.2.4.1 Intergranular Bubbles

Grain boundary bubble growth and coalescence are crucial mechanisms in generating transient FGR. The bubble density depends on the diffusion properties of uranium vacancies and fission gas atoms and is therefore directly related to the fuel temperature. Figure 11 shows the different grain boundary bubble densities as a function of fuel temperature and burnup. A higher fuel temperature results in fewer available grain boundary bubbles as more bubble coalescence takes place. During the temperature transient, the bubble density does not change for all fuel burnups and for high steady-state temperatures. For low irradiation temperatures, the bubble density is reduced once the fuel temperature is close to the terminal temperature because of the activation of diffusion mechanisms. This reduction in bubble density is more significant at lower burnups. Figure 12 shows the fission gas remaining at grain faces during the transient conditions for both irradiation temperatures.

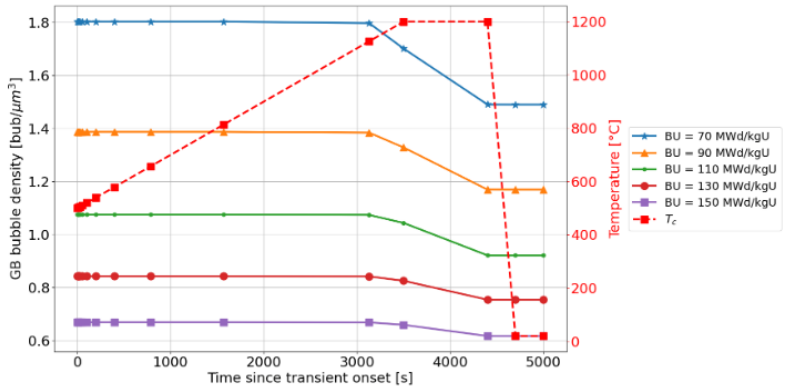

(a) Grain boundary (GB) bubble density during transient at low irradiation temperature

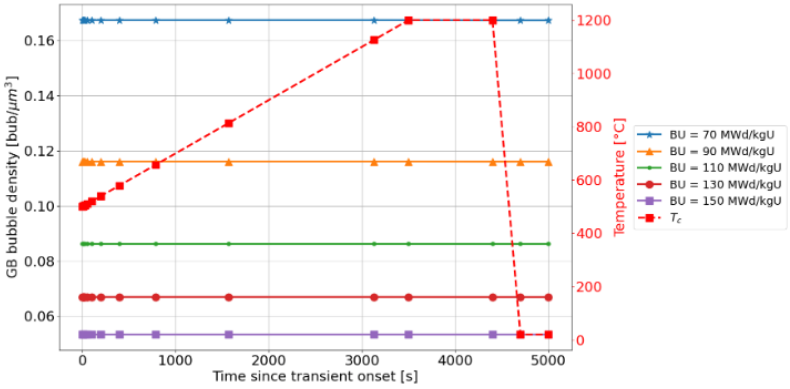

(b) Grain boundary (GB) bubble density during transient at high irradiation temperature

Figure 11. Evolution of intergranular bubble density since onset of transient for irradiation temperatures of 577 (low) and 1,059°C (high).

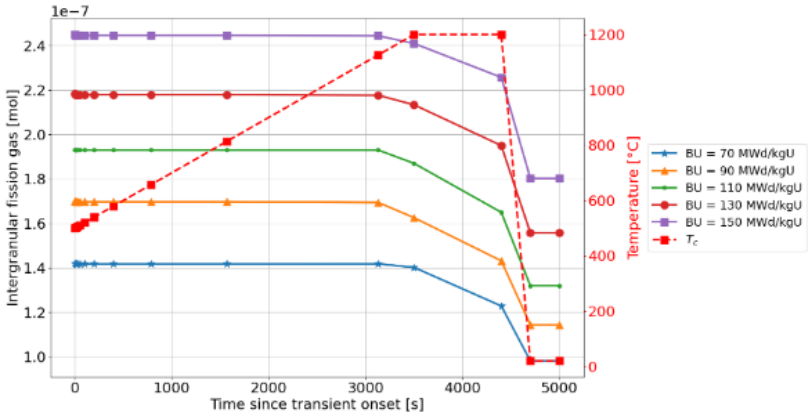

(a) Fission gas at grain boundaries during transient at low irradiation temperature

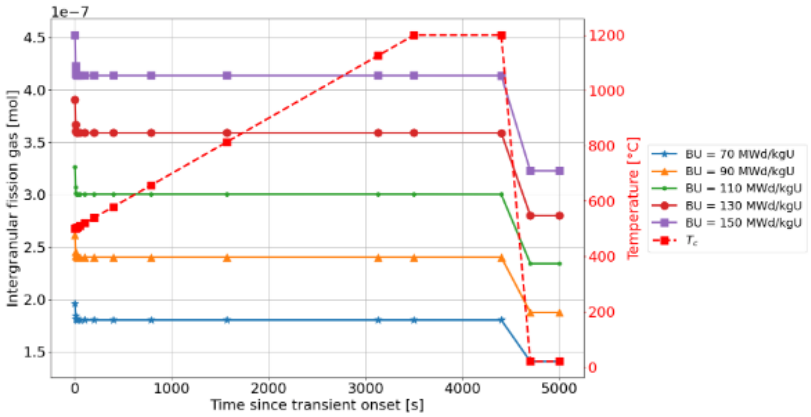

(b) Fission gas at grain boundaries during transient at high irradiation temperature

Figure 12. Evolution of intergranular fission gas since onset of transient for irradiation temperatures of 577 (low) and 1,059°C (high).

Figure 13 shows the corresponding grain boundary bubble pressure. At low irradiation temperature, the intergranular bubble pressure evolves similarly to temperature at a burnup of 110 MWd/kgU or higher. For lower burnup, the model predicts a pressure drop during the hold time at the terminal temperature. The bubble pressure evolution is more consistent with burnup at high irradiation temperature, which follows the temperature evolution by increasing during the ramp, holding at the terminal temperature, and then decreasing during cooldown. Since the pressure is proportional to the temperature, such a trend is expected when the ratio of fission gas atoms to vacancy remains approximately constant. Overall, the predicted pressure is higher than expected in both intragranular and intergranular bubbles.

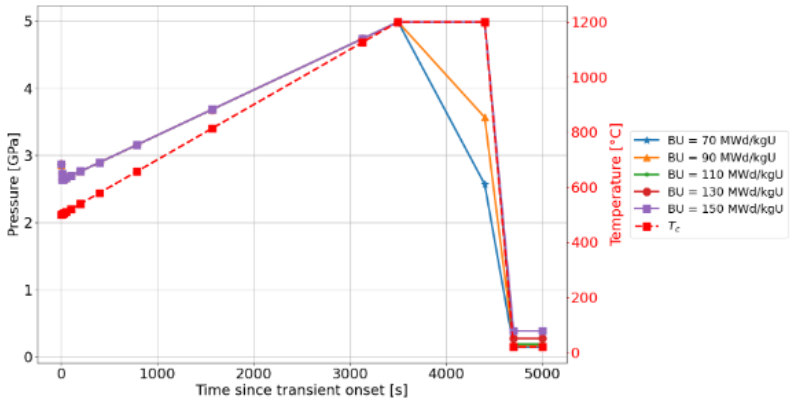

(a) Grain boundary (GB) bubble pressure during transient at low irradiation temperature

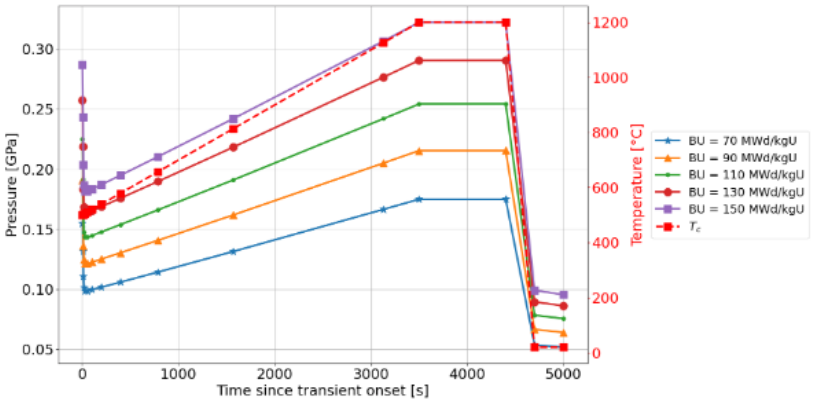

(b) Grain boundary (GB) bubble pressure during transient at high irradiation temperature

Figure 13. Evolution of intergranular bubble pressure since onset of transient for irradiation temperatures of 577 (low) and 1,059°C (high).

4.2.4.2 Intragranular Bubbles

The intragranular bubble density under the temperature transient conditions is shown in Figure 14. In general, once the fuel temperature reaches approximately 1,100°C, high diffusion rates are obtained, which reduces the intragranular bubble density caused by FGR. BISON also predicts that under these conditions intragranular fission gas content remains constant independent of burnup.

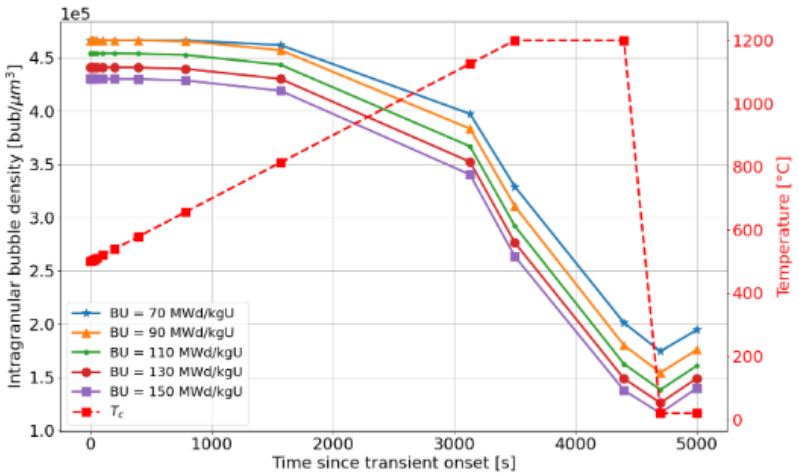

(a) Intragranular bubble density during transient at low irradiation temperature

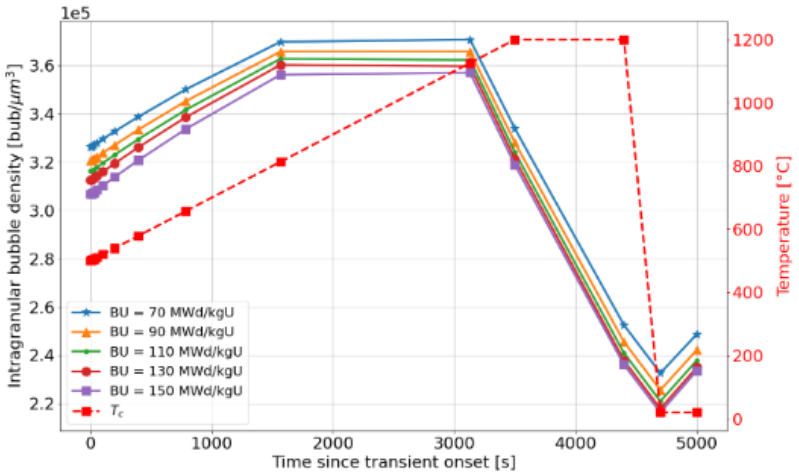

(b) Intragranular bubble density during transient at high irradiation temperature

Figure 14. Evolution of intragranular bubble density since onset of transient for irradiation temperatures of 577 (low) and 1,059°C (high).

4.2.4.3 Porosity

In BISON, fuel porosity depends on the initial porosity after fabrication, the densification rate, and the gaseous porosity. The gaseous porosity is calculated based on the SIFGRS model, which also computes fuel swelling resulting from fission gas bubbles. The gaseous porosity is thus strongly correlated with fission gas behavior, especially once high diffusion rates are reached at fuel temperatures above 1,100°C or when temperature variations cause microcracking. The initial porosity is set to 5%. Only the initial fuel porosity affects the grain boundary bubble density in the model. Figure 15 shows the porosity change during the temperature transient simulation for both temperature cases. At low irradiation temperature, the porosity decreases during the temperature ramp and then increases once the terminal temperature is reached. Finally, a sharp decrease in the porosity is obtained after the cooldown. At high irradiation temperature, the steady-state porosity is higher, and the porosity change with burnup is more significant than the change at low irradiation temperature. At the power shutdown, the porosity initially drops for all

five burnup values. Then, the porosity is mostly constant, with a slight decrease near the terminal temperature, and then drops after the cooldown. Overall, the change in transient fuel porosity is most significant at high irradiation temperature, which can affect transient FGR calculations. This result is consistent with the observed FGR evolution in Figure 4b, in which more FGR is accompanied by a decrease in porosity.

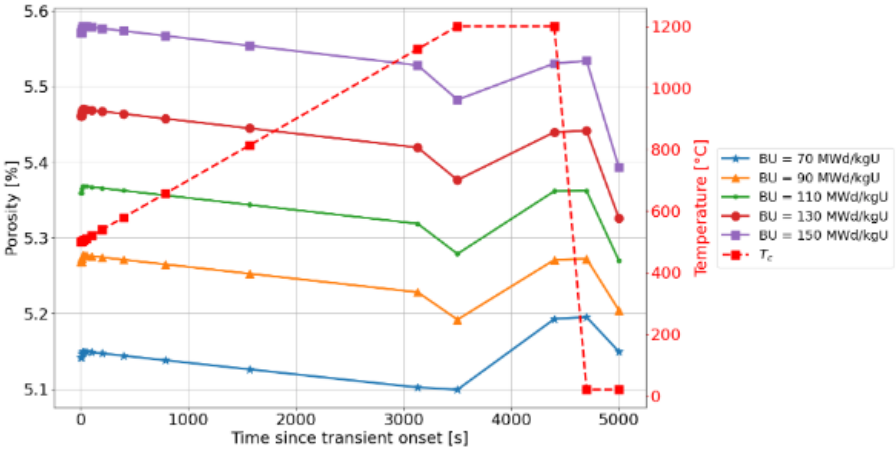

(a) Porosity during transient at low irradiation temperature

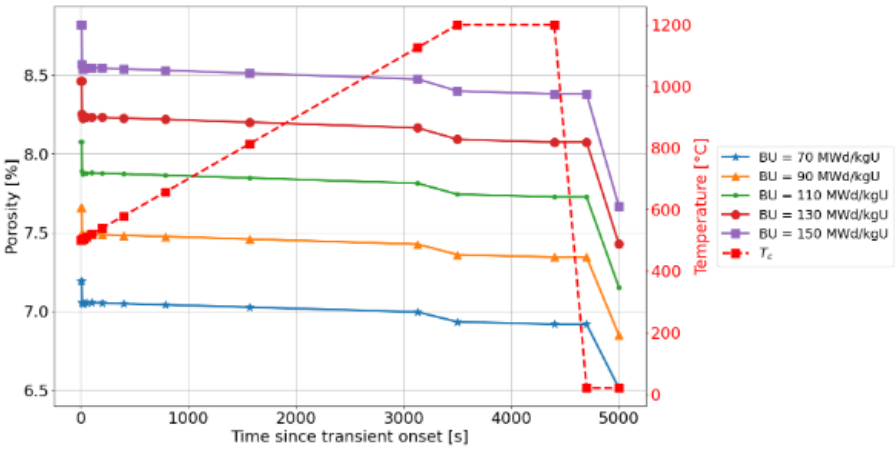

(b) Porosity during transient at high irradiation temperature

Figure 15. Evolution of fuel porosity since onset of transient for irradiation temperatures of 577 (low) and 1,059°C (high).

5. VALIDATION

The transient FGR model in BISON is strongly dependent on temperature variations, which are quite significant during a temperature transient and increase FGR. However, the simulated burst release is not justified by the burst of overpressurized bubbles caused by grain face microcracking but instead by a simplified temperature-dependent model as discussed in Section 3. Although the transient model has

shown promising results when validated against experimental data from LWR fuel rod during ramp tests [23], it generally underestimates the total FGR obtained during the transient. This quantitative assessment shows that the model mainly underestimates FGR during rapid temperature variations.

In this section, BISON's transient FGR model is evaluated and validated against experimental FGR data obtained from the thermal annealing test described in Noirot et al. on a high-burnup UO_2 fuel disk previously irradiated at the Halden Boiling Water Reactor (HBWR) [36]. The relatively slow heating rate of 0.2°C/s used in this experiment and the burnup of 103 GWd/t_{HM} are the key parameters needed to validate the model for high-burnup UO_2.

5.1 Irradiation and Annealing Conditions

The annealing test described in the paper by Noirot et al. [36] used a UO_2 fuel disk extracted from an IFA-649 rod. The rod with an enrichment of 19.77% had been previously irradiated in HBWR to an average burnup of 103 GWd/t_{HM} [36]. The disk's dimensions are larger than those of the MiniFuel, and they correspond to a radius of 4.1 mm and a thickness of 1 mm. In Figure 3 of the paper by Noirot et al. [36], the calculated temperature history is shown for the center disk. The fuel temperature was initially decreasing from approximately 1050°C until it reached nearly 700°C at 35 MWd/kgU, then remained relatively constant for the rest of the irradiation time [36]. However, the power history was not described, so it is estimated for this effort. Noirot et al. [36] report a total FGR of 2.9% after the steady-state irradiation conditions, and they also confirm extensive HBS formation with an average porosity of 11% [36] . Additional experimental observations indicate that the formation of HBS enhanced fission gas retention under steady-state irradiation [36].

An out-of-pile annealing test was performed on the fuel disk. The experimental process raised the sample's temperature to 300°C at 0.5°C/s, held it for 15 minutes, raised it again to 1,200°C at 0.2°C/s, held it again for 15 minutes, and then it was allowed to cool down naturally [36]. The total percentage of fission gas released during the test was 30% [36]. Two FGR peaks were measured: (1) the first peak was obtained between 880 and 1,110°C, and (2) a second peak occurred between 1,110 and 1,200°C, as shown in Figure 9 of the paper by Noirot et al. [36].

5.2 Simulation Setup

Noirot et al. [36] report limited temperature gradients within the fuel disk and provide the maximum temperature history in the disk. Because MiniFuel also has limited temperature gradients and the simulated fuel temperature is controlled to approximately match the experimental disk temperature, the MiniFuel geometry and mesh were used again in the analysis described in this section. The simulated UO_2 disk sample was irradiated under steady-state conditions to a burnup of 103 GWd/t_{HM}, and then a temperature ramp was applied. This approach was slightly different from the experimental setup, in which the temperature transient was applied on previously irradiated fuel. However, since negligible FGR was obtained experimentally during the first ramp to 300°C [36], there was no need to restart the simulation at the onset of the temperature ramp. Instead, the ramp directly followed the steady-state conditions in the simulation, resulting in a drop in the fuel temperature from approximately 700 to 300°C. Figure 3 shows that at approximately 700°C, the initial transient FGR caused by the drop in the fuel temperature following the power shutdown was also negligible. Therefore, it is reasonable to simply apply a LOCA-like abrupt temperature ramp.

For this purpose, the cladding temperature was set to follow an imposed temperature history. Because the power history was not provided, the LHR was set to 250 W/cm based on other power history profiles obtained in HBWR [37]. The LHR remained constant during the entire irradiation time in the simulation.

It was then reduced to 7% for the remaining simulation time. The gap thermal conductivity was reduced to impose a fuel temperature close to 700°C in steady-state conditions, and remained constant due to the constant LHR. The initial drop in the temperature calculated in the paper by Noirot et al. [36] is not accounted for in this work because the power history was not provided. The fission rate density was adjusted to account for the geometry of the HBWR fuel disk, however it remains an approximative value. Note that the fission gas atom diffusivity depends on the fission rate density. However, the steady-state fuel temperature is relatively low for most of the irradiation time; therefore, the fission gas diffusion is limited.

The power shutdown was set to occur 5 seconds after the cladding temperature started to increase which then caused the fuel temperature to approximately match the cladding temperature in a manner similar to that illustrated in the profile shown in Figure 2.

The temperature history can be summarized as follows:

- During steady-state conditions, the cladding temperature was set to 300°C.
- When a burnup of 103 GWd/t_{HM} was reached, the temperature increased up to 1,200°C at 0.2°C/s following the experimental annealing test.
- The temperature was held at 1,200°C for 15 minutes.
- Finally, the temperature was decreased to 20°C in 300 seconds.

The initial fuel porosity was chosen to be 5%, and the initial grain size was set to 18 μm.

5.3 Results

The variation in FGR with burnup during the entire simulation time is shown in Figure 16a. In the steady-state phase, almost no fission gas is released until a high burnup of 63 MWd/kgU is reached. Up to 103 MWd/kgU, the total FGR is close to 7%, which is higher than the experimental value of 2.9%. In the transient phase, the total FGR is about 4.1%, as seen in Figure 16b. The transient total FGR predicted by BISON is also lower than the experimental 30% FGR reproduced in the same figure. A large portion of the fission gas is in fact released during the hold period at 1200°C, which closely matches the temperature at which the highest instantaneous release was observed experimentally [36]. However, the FGR fraction at this peak is largely underestimated by BISON. Compared with the experimental results, BISON's model mainly underestimates the second peak obtained experimentally. Additionally, the first experimental FGR peak is not captured by the model.

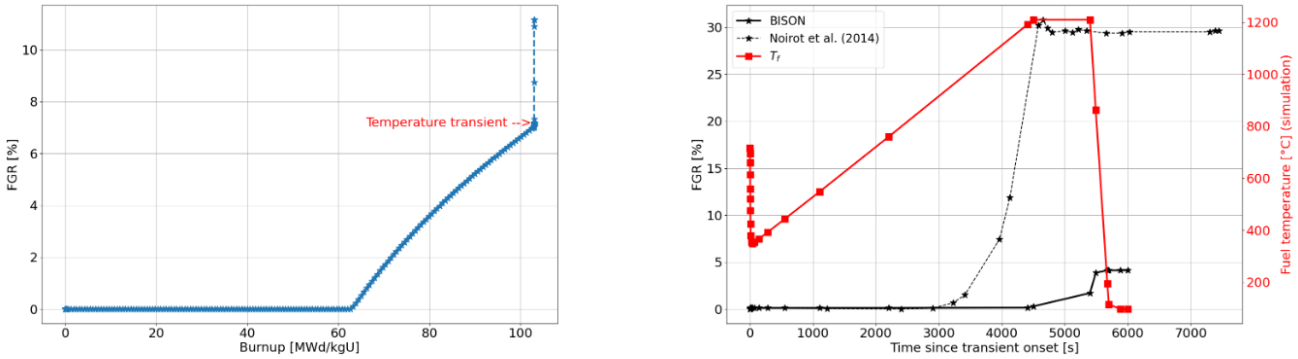

(a) **(b)**

Figure 16. Evolution of FGR with burnup before and during the transient (a) and of FGR during the temperature transient along with fuel temperature. (b).

The model predicts that the variation in intragranular fission gas during the temperature transient is negligible. Figure 17 reveals that most of the released gas was originally located at grain faces. However, despite most FGR coming from grain faces in the model, HBS formation is not accounted for. Since HBS is mainly characterized by large bubbles filled with fission gas and submicron grains, it is very sensitive to microcracking under temperature transients. HBS is considered an attributing factor to the FGR measured in the experimental annealing test [36]. Instead, in this case, most of the fission gas remained inside grains. This is caused by the large grain size, despite the high burnup conditions. Moreover, unlike the fission gas diffusion model, the microcracking model in BISON does not account for the bubble pressure buildup. Figure 18 shows the evolution of the average grain boundary bubble pressure and the radius of curvature during the transient. In addition to the fuel temperature, the ratio of the number of fission gas atoms and of vacancies in grain-face bubbles controls the bubble pressure. The model predicts that the bubble pressure evolution follows the evolution of the fuel temperature during the temperature transient and is constant during the hold time. Moreover, the bubble pressure is on the order of gigapascals, which would typically cause microcracking and subsequent burst during a transient. Finally, the grain boundary bubble radius of curvature starts to increase when the fuel temperature is close to 900°C and goes up sharply during the hold time as intergranular fission gas decreases as shown in Figure 17.

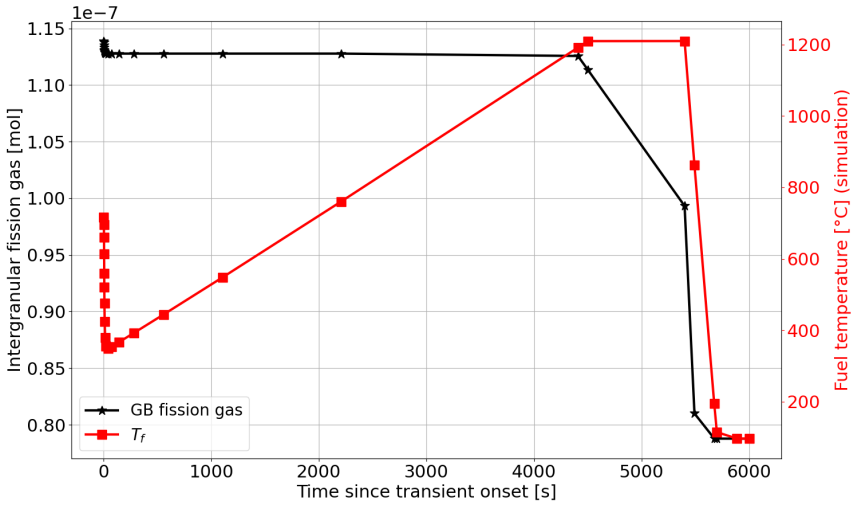

Figure 17. Variation of intergranular fission gas and fuel temperature during the temperature transient.

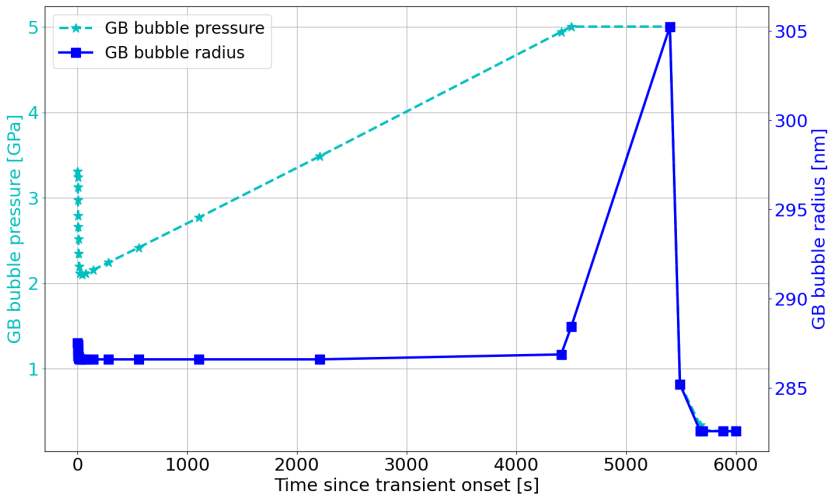

Figure 18. Evolution of the fission gas average bubble pressure and radius of curvature at GB during the transient.

6. DISCUSSION

6.1 Model Performance

The transient FGR model in BISON captures several important aspects of FGR under temperature transient conditions. The irradiation temperature affects the total FGR during the transient phase. A higher steady-state fuel temperature leads to more FGR during the transient as more fission gas accumulates at grain faces, as shown in Table 2. Increasing burnup further increases FGR, independent of temperature. However, the release fraction does not follow the same trend with evolving burnup depending on the fuel temperature. The model shows that at higher heating rates, less FGR is obtained during the transient, which agrees with experimental evidence [10, 12]. Additionally, the model accounts for the effects of the

terminal temperature after the ramp and hold time on fission gas diffusion and release. Both the terminal temperature and hold time affect transient FGR, as noted in the paper by Une et al. [10].

The model includes main microstructural effects on FGR, such as average grain size, UO_2 defect diffusion rates (xenon and uranium vacancy), and chromium dopant addition. The FGR evolution with each of these microstructural effects follows the same trends as those observed experimentally. A larger grain size results in less FGR. Higher xenon diffusion rates slightly increase FGR up to a certain saturation level. The behavior of FGR is not significantly affected by a change in the uranium vacancy diffusion for an enhancement factor of up to 100. Finally, chromium-doped UO_2 is predicted to significantly decrease FGR in steady-state and transient conditions (27 and 6% less FGR, respectively, in the simulated example).

Despite good agreement with experimental data on general trends of FGR evolution under the various conditions explored in Section 4, the model does not perform well when validated against high burnup temperature transient experimental measurements [36]. While the discrepancy in the steady state FGR can be partially attributed to the absence of HBS effects in the model and of experimental data on the LHR, the transient FGR of approximately 4% is still far below the experimentally obtained 30% FGR. A similar result was previously obtained in the paper by Barani et al. [23], where a rapid temperature variation did not result in a significant burst according to BISON's model, in contrast with the experimental data. Therefore, the purely temperature-dependent transient model does not fully represent the fission gas behavior at high burnup, and further model improvements are necessary for validation purposes. However, this is expected because the existing model was developed based on fission gas burst release during power ramps, which is associated with different microscopic mechanisms and, typically, higher fuel temperatures than those considered in this work.

6.2 Potential Improvements

The presence of HBS affects FGR when the fuel undergoes large temperature variations. Accounting for HBS in transient state essentially adds (1) significant reduction in the average grain size, which leads to more FGR, as shown in Figure 9, and (2) the presence of large bubbles of fission gas, which retain a large portion of the total fission gas in the fuel. This last point will also correct the bubble pressure calculation, which will need to be included in the fragmentation-based model. The model would ideally account for a certain threshold pressure in the overpressurized HBS bubbles and would thus produce burst release above such pressure. As pointed out by Une et al. [10], fragmentation develops more as fuel burnup increases, and it also develops with higher heating rates.

6.3 Experimental Test Development

In addition to the necessary additional model development for modeling FGR in temperature transients in BISON, a series of separate-effects irradiation tests on MiniFuel can provide not only better understanding of the FGR mechanisms, but also specific sets of data for validation purposes. Given the successful fabrication and post-irradiation examination of the first MiniFuel vehicle at low burnup, an extension of the irradiation period to achieve higher burnups is of interest, especially to evaluate microstructure evolution under irradiation, fission gas release, and fuel swelling. In addition to higher burnups, FGR at higher fuel temperatures, representative of an LWR fuel centerline temperature, needs to be investigated. In fact, in the previously discussed MiniFuel irradiation tests, the target fuel temperature is around 500°C [2, 4] similarly to the fuel temperature at the rim region in LWR normal conditions [11]. The decoupling of fuel temperature from the fission rate allows for a separate-effects study similar to the modeling efforts presented in this work.

Based on the qualitative evaluation of FGR in BISON at different irradiation temperatures and burnups, the UO_2 MiniFuel test matrix shown in Table 5 is proposed to help to further develop and validate the FGR model under both steady-state and transient conditions. The suggested irradiation temperatures are expected to result in significantly more FGR as a result of the enhanced fission gas diffusion and are closer to a typical LWR fuel centerline temperature. Two samples per irradiation temperature are proposed to examine the fuel microstructure after irradiation and to perform a temperature transient test to evaluate transient FGR. The samples irradiated up to 80 MWd/kgU are proposed to evaluate the effects of burnup and of the expected HBS development on FGR (particularly at the lowest irradiation temperature), which will be compared to that of the samples at 40 MWd/kgU. While this test matrix targets UO_2, similar conditions can be applied to doped UO_2 for comparison.

Table 5. Proposed UO_2 MiniFuel test matrix.

Target	Burnup [MWd/kgU]	Irradiation Temperature [°C] (2 samples per temperature)
Target 1 (6 capsules)	40	900, 1100, 1300
Target 2 (6 capsules)	80	900, 1100, 1300

7. CONCLUSION

The application of transient conditions in UO_2 fuels significantly affects the amount of released fission gas to the plenum volume in a fuel rod. The fuel performance code BISON can model FGR in UO_2 and doped UO_2 fuels. The BISON FGR model includes physics-based diffusion-controlled FGR calculations in addition to fully temperature-dependent microcracking-based FGR; the latter component was originally developed based on experimental results from power ramp tests. In this report, the model was exercised and evaluated under several temperature transient scenarios to fully assess its capabilities. BISON accounts well for the effects of temperature conditions and microstructural features on diffusion-controlled FGR. However, the model, which does not yet include a representation of FGR driven by fuel fragmentation during LOCA-type transients, largely underestimates transient FGR in the considered transient cases when compared with experimental data.

Two major mechanisms behind the experimentally observed fission gas burst release are currently not accounted for in the model. First, the formation of HBS results in a significant drop in the average grain size, allowing for more fission gas at grain faces because of shorter diffusion times. Second, the overpressurization of HBS bubbles leads to important fragmentation during large and rapid temperature variations. Therefore, further model development in BISON is necessary to better capture transient FGR. Moreover, further irradiation experiments on UO_2 MiniFuel specimen at higher burnups and fuel temperatures will provide valuable validation means for BISON's FGR model.

8. REFERENCES

[1] C. M. Petrie, J. R. Burns, A. M. Raftery, A. T. Nelson, and K. A. Terrani, "Separate effects irradiation testing of miniature fuel specimens," *J. Nucl. Mater.*, vol. 526, p. 151783, 2019, doi: 10.1016/j.jnucmat.2019.151783.

[2] J. M. Harp, R. N. Morris, C. M. Petrie, J. R. Burns, and K. A. Terrani, "Postirradiation examination from separate effects irradiation testing of uranium nitride kernels and coated particles," *J. Nucl. Mater.*, vol. 544, p. 152696, 2021, doi: 10.1016/j.jnucmat.2020.152696.

[3] C. M. Petrie, J. R. Burns, R. N. Morris, K. R. Smith, A. G. Le Coq, and K. A. Terrani, "Irradiation of Miniature Fuel Specimens in the High Flux Isotope Reactor," *Oak Ridge Natl. Lab. Rep.*, p. ORNL/SR-2018/874, 2018, [Online]. Available: https://www.osti.gov/servlets/purl/1458354.

[4] C. M. Petrie *et al.*, "Monolithic ATF MiniFuel Sample Capsules Ready for HFIR Insertion," 2020, doi: 10.2172/1615787.

[5] A. M. Raftery *et al.*, "Development of a characterization methodology for post-irradiation examination of miniature fuel specimens," *Oak Ridge Natl. Lab. Rep.*, p. ORNL/SPR-2018/918, 2018, [Online]. Available: https://www.osti.gov/servlets/purl/1474563.

[6] A. Scolaro, P. Van Uffelen, C. Fiorina, A. Schubert, I. Clifford, and A. Pautz, "Investigation on the effect of eccentricity for fuel disc irradiation tests," *Nucl. Eng. Technol.*, vol. 53, no. 5, pp. 1602–1611, 2020, doi: 10.1016/j.net.2020.11.003.

[7] D. R. Olander, "Fundamental aspects of nuclear reactor fuel elements," United States, 1976. [Online]. Available: http://inis.iaea.org/search/search.aspx?orig_q=RN:08284120.

[8] D. A. Andersson *et al.*, "Multiscale simulation of xenon diffusion and grain boundary segregation in UO2," *J. Nucl. Mater.*, vol. 462, pp. 15–25, 2015, doi: 10.1016/j.jnucmat.2015.03.019.

[9] C. T. Walker, P. Knappik, and M. Mogensen, "Concerning the development of grain face bubbles and fission gas release in UO2 fuel," *J. Nucl. Mater.*, vol. 160, no. 1, pp. 10–23, 1988, doi: 10.1016/0022-3115(88)90003-7.

[10] K. Une, S. Kashibe, and A. Takagi, "Fission gas release behavior from high burnup uo2 fuels under rapid heating conditions," *J. Nucl. Sci. Technol.*, vol. 43, no. 9, pp. 1161–1171, 2006, doi: 10.1080/18811248.2006.9711208.

[11] V. V. Rondinella and T. Wiss, "The high burn-up structure in nuclear fuel," *Mater. Today*, vol. 13, no. 12, pp. 24–32, 2010, doi: 10.1016/S1369-7021(10)70221-2.

[12] Y. Pontillon *et al.*, "Experimental and theoretical investigation of fission gas release from UO2 up to 70 GWd/t under simulated LOCA type conditions: The GASPARD program," *Proc. 2004 Int. Meet. LWR Fuel Perform.*, no. January, pp. 490–499, 2004.

[13] J. P. Hiernaut *et al.*, "Fission product release and microstructure changes during laboratory annealing of a very high burn-up fuel specimen," *J. Nucl. Mater.*, vol. 377, no. 2, pp. 313–324, 2008, doi: 10.1016/j.jnucmat.2008.03.006.

[14] M. Marcet *et al.*, "In situ characterization of UO2 microstructure changes during an annealing test in an environmental scanning electron microscope," *Mater. Res. Soc. Symp. Proc.*, vol. 1215, no. January, pp. 157–162, 2010, doi: 10.1557/proc-1215-v16-44.

[15] G. Pastore *et al.*, "Uncertainty and sensitivity analysis of fission gas behavior in engineering-scale fuel modeling," *J. Nucl. Mater.*, vol. 456, pp. 398–408, 2015, doi: https://doi.org/10.1016/j.jnucmat.2014.09.077.

[16] R. L. Williamson *et al.*, "Multidimensional multiphysics simulation of nuclear fuel behavior," *J. Nucl. Mater.*, vol. 423, no. 1–3, pp. 149–163, 2012, doi: 10.1016/j.jnucmat.2012.01.012.

[17] J. D. Hales *et al.*, "BISON Theory Manual The Equations behind Nuclear Fuel Analysis," 2016, doi: 10.2172/1374503.

[18] D. Gaston, C. Newman, G. Hansen, and D. Lebrun-Grandié, "MOOSE: A parallel computational framework for coupled systems of nonlinear equations," *Nucl. Eng. Des.*, vol. 239, no. 10, pp. 1768–1778, 2009, doi: 10.1016/j.nucengdes.2009.05.021.

[19] R. L. Williamson, G. Pastore, S. R. Novascone, B. W. Spencer, and J. D. Hales, "Modelling of LOCA Tests with the BISON Fuel Performance Code," 2016, [Online]. Available: https://inldigitallibrary.inl.gov/sites/sti/sti/7146879.pdf.

[20] R. L. Williamson *et al.*, "Validating the BISON fuel performance code to integral LWR experiments," *Nucl. Eng. Des.*, vol. 301, pp. 232–244, 2016, doi: https://doi.org/10.1016/j.nucengdes.2016.02.020.

[21] K. A. Gamble *et al.*, "Modeling and Simulation Transactions of the American Nuclear Society , Vol . 112 , San Antonio , Texas , June 7 – 11 , 2015 Modeling and Simulation," vol. 112, 2015.

[22] G. Pastore, D. Pizzocri, J. D. Hales, S. R. Novascone, R. L. Williamson, and B. W. Spencer, "Modeling of transient fission gas behavior in oxide fuel and application to the BISON code," *Proc. Enlarg. Halden Program. Gr. Meet. Roros, Norw.*, no. May 2015, pp. 12–16, 2014.

[23] T. Barani *et al.*, "Analysis of transient fission gas behaviour in oxide fuel using BISON and TRANSURANUS," *J. Nucl. Mater.*, vol. 486, pp. 96–110, 2017, doi: 10.1016/j.jnucmat.2016.10.051.

[24] U. Katsumi and K. Shinji, "Fission gas release during post irradiation annealing of bwr fuels," *J. Nucl. Sci. Technol.*, vol. 27, no. 11, pp. 1002–1016, 1990, doi: 10.1080/18811248.1990.9731285.

[25] G. Pastore, L. Luzzi, V. Di Marcello, and P. Van Uffelen, "Physics-based modelling of fission gas swelling and release in UO2 applied to integral fuel rod analysis," *Nucl. Eng. Des.*, vol. 256, pp. 75–86, 2013, doi: https://doi.org/10.1016/j.nucengdes.2012.12.002.

[26] T. J. Gerczak, C. M. Parish, P. D. Edmondson, C. A. Baldwin, and K. A. Terrani, "Restructuring in high burnup UO2 studied using modern electron microscopy," *J. Nucl. Mater.*, vol. 509, pp. 245–259, 2018, doi: 10.1016/j.jnucmat.2018.05.077.

[27] J. Noirot, L. Desgranges, and J. Lamontagne, "Detailed characterisations of high burn-up structures in oxide fuels," *J. Nucl. Mater.*, vol. 372, no. 2–3, pp. 318–339, 2008, doi: 10.1016/j.jnucmat.2007.04.037.

[28] J. B. Ainscough, B. W. Oldfield, and J. O. Ware, "Isothermal grain growth kinetics in sintered UO2 pellets," *J. Nucl. Mater.*, vol. 49, no. 2, pp. 117–128, 1973, doi: 10.1016/0022-3115(73)90001-9.

[29] S. Yajima, H. Furuya, and T. Hirai, "Lattice and grain-boundary diffusion of uranium in UO2," *J. Nucl. Mater.*, vol. 20, no. 2, pp. 162–170, 1966, doi: 10.1016/0022-3115(66)90004-3.

[30] H. Matzke, "Atomic transport properties in UO2 and mixed oxides (U, Pu)O2," *J. Chem. Soc. Faraday Trans. 2 Mol. Chem. Phys.*, vol. 83, no. 7, pp. 1121–1142, 1987, doi: 10.1039/F29878301121.

[31] D. A. Andersson, B. P. Uberuaga, P. V Nerikar, C. Unal, and C. R. Stanek, "U and Xe transport in $UO_{2\pm x}$: Density functional theory calculations," *Phys. Rev. B*, vol. 84, no. 5, p. 54105, Aug. 2011, doi: 10.1103/PhysRevB.84.054105.

[32] J. A. Turnbull, R. White, and C. Wise, "The diffusion coefficient for fission gas atoms in uranium dioxide," *Water React. Fuel Elem. Comput. Model. Steady State, Transient Accid. Cond.*, pp. 174–181, 1989.

[33] J. Arborelius *et al.*, "Advanced doped UO2 pellets in LWR applications," *J. Nucl. Sci. Technol.*, vol. 43, no. 9, pp. 967–976, 2006, doi: 10.1080/18811248.2006.9711184.

[34] M. W. D. Cooper, C. R. Stanek, and D. A. Andersson, "The role of dopant charge state on defect chemistry and grain growth of doped UO2," *Acta Mater.*, vol. 150, pp. 403–413, 2018, doi: 10.1016/j.actamat.2018.02.020.

[35] M. W. D. Cooper, C. R. Stanek, and A. D. R. Andersson, "Milestone Report: Calculate parameters controlling grain growth in doped UO2 [M3MS-18LA0201035]," 2018, doi: 10.2172/1457319.

[36] J. Noirot, Y. Pontillon, S. Yagnik, J. A. Turnbull, and T. Tverberg, "Fission gas release behaviour of a 103 GWd/tHM fuel disc during a 1200 C annealing test," *J. Nucl. Mater.*, vol. 446, no. 1–3, pp. 163–171, 2014, doi: 10.1016/j.jnucmat.2013.12.002.

[37] J. A. Turnbull, "Review of Nuclear Fuel Experimental Data," *Organ. Econ. Co-operation Dev. - Nucl. Energy Agency*, no. January, 1995.